

---

# FTS: A FRAMEWORK TO FIND A FAITHFUL TIME SIEVE

---

**Songning Lai\***  
HKUST(GZ)

Deep Interdisciplinary Intelligence Lab (*DI<sup>2</sup>Lab*)  
songninglai@hkust-gz.edu.cn

**Ninghui Feng\***  
HKUST(GZ)

ninghuifeng@hkust-gz.edu.cn

**Jiechao Gao**  
Virginia University  
jg5ycn@virginia.edu

**Hao Wang**  
CMU  
hao2@alumni.cmu.edu

**Haochen Sui**  
University of Michigan  
hcsui@umich.edu

**Xin Zou**  
HKUST(GZ)  
xinzou@hkust-gz.edu.cn

**Jiayu Yang**  
HKUST(GZ)  
jyang729@connect.hkust-gz.edu.cn

**Wenshuo Chen**  
Shandong Univeristy  
chatoncws@gmail.com

**Hang Zhao, Xuming Hu**  
HKUST(GZ)  
{hangzhao, xuminghu}@hkust-gz.edu.cn

**Yutao Yue<sup>†</sup>**  
HKUST(GZ)  
Institute of Deep Perception Technology, JITRI  
Deep Interdisciplinary Intelligence Lab (*DI<sup>2</sup>Lab*)  
{yutaoyue}@hkust-gz.edu.cn

## ABSTRACT

The field of time series forecasting has garnered significant attention in recent years, prompting the development of advanced models like TimeSieve, which demonstrates impressive performance. However, an analysis reveals certain unfaithfulness issues, including high sensitivity to random seeds, input and layer noise perturbations and parametric perturbations. Recognizing these challenges, we embark on a quest to define the concept of **Faithful TimeSieve (FTS)**, a model that consistently delivers reliable and robust predictions. To address these issues, we propose a novel framework aimed at identifying and rectifying unfaithfulness in TimeSieve. Our framework is designed to enhance the model's stability and faithfulness, ensuring that its outputs are less susceptible to the aforementioned factors. Experimentation validates the effectiveness of our proposed framework, demonstrating improved faithfulness in the model's behavior.

**Keywords** Time series · Faithfulness · Robustness

## 1 Introduction

Time series forecasting is a well-established learning problem that involves analyzing time series data to predict future trends based on historical information [1, 2]. The field of time series forecasting has witnessed remarkable growth, with a multitude of advanced models [3, 4, 5, 6] emerging to push the boundaries of predictive capabilities. In this context, Feng et al. have developed TimeSieve [7], a state-of-the-art model that integrates wavelet transform [8, 9, 10] and information bottleneck theory [11]. TimeSieve incorporates recent advancements in the field, resulting in superior performance and offering novel insights, and TimeSieve outperforms other advanced models [12, 13, 14, 15].

---

\*The first two authors contributed equally to this work.

<sup>†</sup>Correspondence to Yutao Yue {yutaoyue@hkust-gz.edu.cn}

While TimeSieve demonstrates impressive performance, it also exhibits instability when confronted with perturbations. Specifically, during our experimentation, we observed substantial variability influenced by perturbations in random seeds, with differences of up to 50%. To illustrate this issue, we conducted training using five random seeds, designating one of the trained models as the baseline. We then compared the test results of the remaining four models with those of the baseline model to calculate the percentage of variation. Moreover, we introduced a small perturbation to the test set inputs ( $x(t)' = x(t) + \mathcal{N}(0, \sigma)$ , where  $\sigma = 0.1$  represents a perturbation of a certain radius), and the experimental outcomes revealed a performance change or decrease of about 30%. These issues can significantly undermine the fidelity of the model.

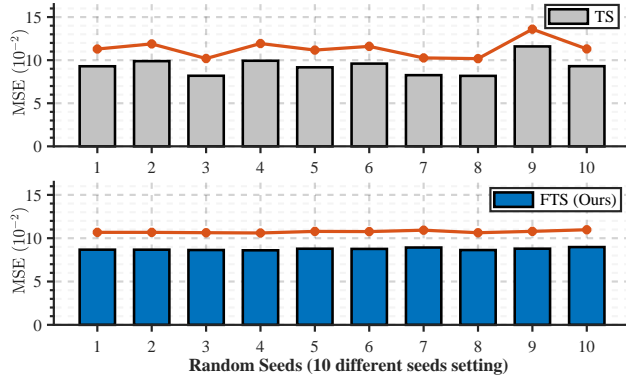


Figure 1: Ten different random seeds are selected to train TimeSieve (TS) and Faithful TimeSieve (FTS) respectively.

To address the issues of faithfulness in TimeSieve, a precise definition is required: what constitutes a **Faithful TimeSieve (FTS)**? We propose that a FTS encompasses three key attributes:

(i) **Similarity in IB Space (Sib)**. This attribute pertains to preserving essential information between the original time series and its filtered representation in the Information Bottleneck (IB) space. The filtering process involves applying the TimeSieve model to the original coefficients, resulting in filtered coefficients denoted as  $\hat{\pi}_i$ . To satisfy this attribute, the overlap between the original coefficients  $\pi_i$  and the disturbed coefficients  $\hat{\pi}_i$ , denoted as  $D_1(\hat{\pi}_i, \pi_i)$ , must exceed a predefined threshold  $\beta$ . This ensures that the filtering process retains the crucial information necessary for accurate predictions.

(ii) **Consistency in Prediction Space (Cps)**. This attribute focuses on the quality of predictions made using the original weights  $\omega$  compared to those made using the fine-tuned weights  $\tilde{\omega}$ . The forecasts, denoted as  $y(x(t), \omega)$  and  $y(x(t), \tilde{\omega})$ , respectively, are based on the original and fine-tuned outputs. The attribute requires that the difference between these two forecasts, measured by a suitable distance metric  $D$  denoted as  $D_2$ , is bounded by a constant  $\alpha_1$ . In other words, the predictive accuracy of the TimeSieve model should not significantly degrade when using the fine-tuned weights instead of the original weights.

(iii) **Stability in Noise Perturbations (Snp)**. This attribute addresses the robustness of the TimeSieve model’s predictions to perturbations. It ensures that the model’s forecasts remain stable when be perturbed within a certain range. Specifically, the difference between the forecast  $y(x(t), \tilde{\omega})$  based on the original outputs and the forecast  $y(x(t) + \delta, \tilde{\omega})$  when the input is perturbed by a small amount  $\delta$ , should be bounded by a constant  $\alpha_2$ . This attribute guarantees that the TimeSieve model’s predictions exhibit limited sensitivity to perturbations in the input or the model’s internal state, thus maintaining stability.

In this study, we make the following key contributions:

- (1) **Faithfulness Analysis of TimeSieve:** We conduct a comprehensive analysis to identify and understand the inherent challenges to faithfulness in the TimeSieve model. This analysis provides valuable insights into the limitations of the model and the factors that affect its fidelity to the original time series.
- (2) **Definition of Faithful TimeSieve:** We propose a rigorous definition for a Faithful TimeSieve, outlining the essential attributes that ensure the model’s robustness and stability. These attributes serve as a guideline for evaluating and enhancing the faithfulness of TimeSieve.
- (3) **Framework for Finding Faithful TimeSieve:** To address the identified faithfulness issues, we develop a novel framework that integrates strategies to mitigate these challenges while preserving the model’s performance. The framework aims to enhance the fidelity of TimeSieve by incorporating techniques that maintain the defined attributes of a Faithful TimeSieve.

(4) **Framework Validation and Proof:** Through extensive proof of FTS’s bounds mathematically and experimentation, we demonstrate the effectiveness of our framework in improving the faithfulness of TimeSieve. The results validate the practical utility and theoretical soundness of our approach.

## 2 Related Work

### 2.1 Time Series Forecasting

Over the past few years, significant advancements have been made in the field of time series forecasting, leading to the development of several effective forecasting models. Many of these innovative models leverage Multi-Layer Perceptrons (MLPs) to harness their powerful capabilities. Examples of such models include the MSD-Mixer [16], DLinear [17], and FreTs [6]. These MLP-based models utilize sophisticated data manipulations and learning strategies to improve their forecasting performance. Simultaneously, Transformer architectures have also gained considerable prominence in time series forecasting. Models such as PatchTST [3] and the memory-efficient Informer [18] have proven to be highly effective in capturing temporal dependencies through advanced data transformation techniques. These Transformer-based models excel at extracting meaningful patterns from time series data by leveraging their ability to model long-range dependencies and capture intricate relationships.

In recent work - TimeSieve , Feng et al.[7] have introduced an innovative approach that integrates wavelet transform with contemporary machine learning methodologies and information bottleneck theory for time series forecasting. The experimental evaluation of TimeSieve demonstrates its effectiveness compared to existing models. By evaluating the model on diverse time series datasets, TimeSieve presents significant improvements in forecasting accuracy and robustness. These results showcase the potential of integrating wavelet transform and information bottleneck theory with contemporary machine learning techniques, opening up new avenues for advancing time series forecasting research.

### 2.2 Faithful Time Series

The challenge of achieving faithful time series prediction, which is crucial for numerous applications, has been a longstanding issue [19, 20, 21]. Previous research has tackled this problem by proposing more faithful conventional prediction methods [22, 23, 24, 25, 26, 27] based on auto-regression, aiming to mitigate the impact of noise. Another line of work focuses on the training data [28] and explores techniques such as data perturbation to alleviate bias [29]. In recent years, deep learning has gained attention for time series prediction. However, deep learning models are often sensitive and prone to overfitting, particularly in the presence of outliers. Recent studies propose various improvements in model training to address these challenges. Approaches such as teacher forcing [30], specialized loss functions [31], model ensembles [32, 33], as well as data denoising [34], data augmentation [35], data decomposition [36], and data compensation [37] have been explored to enhance model generalization and train models with more reliable datasets. Among these efforts, Cheng et al. [38] proposed DARF, which leverages adversarial learning to capture correlations across multiple time series and reduce data bias. Zhang et al. [39] introduced localized stochastic sensitivity (LSS) minimization for Recurrent Neural Networks (RNNs) to reduce output sensitivities. TimeX [40] presents a time series model that enhances model faithfulness by introducing model behavior consistency. Yu et al. [41] propose a decomposition-based Transformer to improve the predictability of Transformers.

These studies demonstrate the significant potential of learning-based models in robust time series prediction. However, they lack a unified framework and do not explicitly focus on the definition of "faithfulness" itself, which poses challenges in evaluation and interpretation. To address these limitations, our work aims to provide a comprehensive and unified framework for achieving faithful time series prediction. We recognize the importance of visual attention on the definition of faithfulness, enabling a more thorough understanding and evaluation of the models. By integrating key insights from previous works and leveraging advanced techniques, our proposed framework aims to enhance the faithfulness of time series prediction in a principled and interpretable manner.

## 3 Method

### 3.1 Preliminaries: TimeSieve

TimeSieve [7] is a novel time series forecasting model that combines the strengths of wavelet transform and the information bottleneck theory to enhance prediction performance.

#### Wavelet Decomposition and Reconstruction

The Wavelet Decomposition Block (WDB) decomposes the input time series  $x(t) \in \mathbb{R}^{T \times C}$  into  $\pi_a$  and  $\pi_d$  using wavelet transform, where the approximation coefficients  $\pi_a$  representing the low-frequency trends, and the detail coefficients  $\pi_d$  representing the high-frequency details:

$$\pi_a = \int_{-\infty}^{\infty} x(t)\phi(t)dt, \quad \pi_d = \int_{-\infty}^{\infty} x(t)\psi(t)dt, \quad (1)$$

where  $\phi(t)$  and  $\psi(t)$  are the scaling function and wavelet function, respectively, defined as follows:

$$\phi(t+1) = \sum_{k=1}^N a_k \phi(2t-k), \quad \psi(t+1) = \sum_{k=1}^M b_k \phi(2t-k), \quad (2)$$

Here,  $a_k$  and  $b_k$  are the filter coefficients for the scaling and wavelet functions, respectively, and  $k$  is the index of the coefficients.

This decomposition allows for the extraction of both trend and details from the data. The WRB then reconstructs the time series from the processed coefficients and the reconstructed time series is passed through a simple MLP network for the final prediction:

$$y = MLP\left(\sum \hat{\pi}_a \phi(t) + \sum \hat{\pi}_d \psi(t)\right), \quad (3)$$

where  $\hat{\pi}_a$  and  $\hat{\pi}_d$  denote the filtered approximation and detail coefficients respectively.

### Information Filtering and Compression

The Information Filtering and Compression Block (IFCB) employs the IB principle to filter noise and retain essential information. The objective is to minimize the mutual information  $I(\pi_i; z)$  while maximizing  $I(z; \hat{\pi}_i)$ , where  $\pi_i$  represents the input coefficients,  $\hat{\pi}_i$  are the filtered coefficients, and  $z$  is the intermediate hidden layer and use  $\hat{\pi}_i$ , where  $i \in \{a, d\}$ . The optimization problem is formulated as:

$$\min\{I(\pi_i; z) - \beta \cdot I(z; \hat{\pi}_i)\}, \quad (4)$$

where  $\beta$  is the trade-off parameter. The IFCB uses a deep neural network with a Gaussian distribution for  $p(z|i)$  and a decoder function  $f(z; \theta_d)$  to predict  $\hat{\pi}_i$ . The loss function for training combines the original prediction loss and the IB loss:

$$\mathcal{L}_{IB} = D_{KL}[\mathcal{N}(\mu_z, \Sigma_z) || \mathcal{N}(0, I)] + D_{KL}[p(z) || p(z|i)], \quad (5)$$

$$\mathcal{L} = \mathcal{L}_{reg} + \mathcal{L}_{IB}, \quad (6)$$

where  $\mathcal{L}_{reg}$  is the regression loss, and  $\mathcal{L}_{IB}$  is the IB loss. More details can be seen in this full paper [7].

The contemporary SOTA model TimeSieve, has made significant strides in time series forecasting by effectively harnessing wavelet transform for multi-scale feature extraction and the IB method for noise reduction, but they are not without limitations. Despite their improved predictive performance, this model exhibits a certain fragility when confronted with external disturbances or unforeseen perturbations in the data and parameters. This lack of robustness and stability can lead to suboptimal performance, particularly in dynamic environments where data characteristics may shift with random seeds and other perturbations.

### 3.2 Faithfulness Issues in TimeSieve

The SOTA TimeSieve model, despite its predictive prowess, displays vulnerabilities in the form of sensitivity to random seeds, input perturbations and parameters perturbations, leading to inconsistent performance. These limitations question its faithfulness and suitability for real world scenarios where robustness is crucial. Our focus is on addressing TimeSieve’s instability as a representative case, with the goal of improving trustworthiness in time series forecasting models.

By targeting these challenges, we aim to generalize our proposed solution, extending its applicability beyond TimeSieve to a broader spectrum of models. This endeavor seeks to contribute to the advancement of more reliable and robust forecasting methods, enhancing the overall confidence in time series predictions for various applications.

### 3.3 What Is "faithful time series forecasting" ?

A "faithful time series forecasting" refers to a forecasting model that consistently captures the underlying dynamics of time series data, providing accurate and robust predictions across diverse scenarios. This type of model exhibits resilience to random seeds, input perturbations and parameters perturbations, maintaining its performance over time and remaining insensitive to changes in initialization conditions. By generating stable predictions and offering coherent explanations, a faithful model instills trust, making it highly reliable for real world applications and contributing to our understanding of complex temporal patterns [42, 43, 44].

When discussing "faithful time series forecasting" we emphasize the model's ability to consistently and reliably capture the data's dynamics, thereby ensuring accurate and stable predictions across various scenarios. A faithful forecasting model demonstrates robustness in the face of perturbations in the input data, such as outliers or minor variations, while maintaining its predictive performance as the data evolves over time. It is essential for such a model to be insensitive to changes in initialization conditions, such as random seeds and parameter perturbations, while still extracting meaningful patterns from the data.

The concept of "faithful time series forecasting" places particular emphasis on the model's capacity to generate predictions that remain consistent and coherent, even in the presence of input data perturbations or modifications to the model's architecture or parameters. This stability ensures that the model's explanations of its predictions remain valid and trustworthy, enabling users to rely on its forecasts with confidence. By focusing on the development of faithful time series forecasting models, we can deepen our understanding of complex temporal patterns and enhance the applicability of these models in real world settings.

### 3.4 Definition for FTS

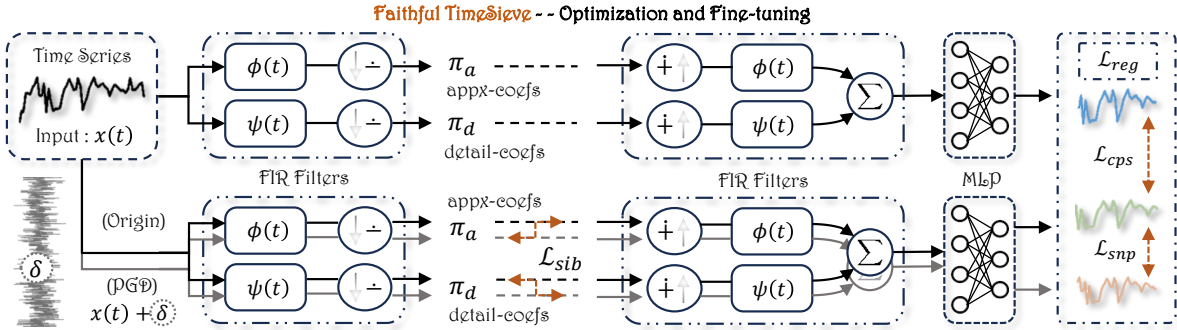


Figure 2: Framework of our proposed Faithful TimeSieve (FTS).

**Definition 1 (Faithful TimeSieve).** A TimeSieve model is considered  $(\alpha_1, \alpha_2, \beta, \delta, R_1, R_2)$ -Faithful if it satisfies the following three attributes for any input time series  $x(t)$  and we want to get  $\tilde{\omega}$  which is a Faithful TimeSieve's weights:

- (i) **Similarity in IB Space (Sib):**

$$\begin{aligned} D_1(\hat{\pi}_a(x(t)), \hat{\pi}_a(x(t) + \delta)) &\leq \beta \text{ for all } \|\delta\| \leq R_1 \text{ and} \\ D_1(\hat{\pi}_d(x(t)), \hat{\pi}_d(x(t) + \delta)) &\leq \beta \text{ for all } \|\delta\| \leq R_1, \text{ where } D_1 \text{ represents some probability distance or divergence,} \\ \|\cdot\| &\text{ denotes a norm and } R_1 \geq 0 \text{ for all } \|\delta\| \leq R_1. \end{aligned}$$

- (ii) **Consistency in Prediction Space (Cps):**

$$D_2(y(x(t), \tilde{\omega}), y(x(t), \omega)) \leq \alpha_1 \text{ for some } \alpha_1 \geq 0, \text{ where } D_2 \text{ is some probability distance or divergence, } \omega \text{ is the weights of the original TimeSieve and } \tilde{\omega} \text{ is the weights of the fine-tuned model.}$$

- (iii) **Stability in Noise Perturbations (Snp):**

$$D_3(y(x(t), \tilde{\omega}), y(x(t) + \delta, \tilde{\omega})) \leq \alpha_2 \text{ for all } \|\delta\| \leq R_2, \text{ where } D_3 \text{ is probability distance or divergence, } \|\cdot\| \text{ is a norm and } R_2 \geq 0,$$

A TimeSieve model, characterized by its unwavering fidelity, is distinguished by its sustained predictive accuracy and stability under perturbations in input data or intrinsic model dynamics, drawing inspiration from referenced as [42].

#### Forecasting Consistency in TimeSieve.

The similarity between forecasts from original and fine-tuned coefficients is quantified by  $\alpha_1$ , measuring the distance  $D$  between  $y(x(t), \tilde{\omega})$  and  $y(x(t), \omega)$ . An ideal scenario is  $\alpha_1 = 0$ , indicating identical forecasts. Our goal is to minimize  $\alpha_1$  for high forecast consistency.

### Stability in TimeSieve.

The stability criterion is defined by  $R_2$  and  $\alpha_2$ , with  $R_2$  being the robustness radius and  $\alpha_2$  the stability level. A model is highly stable if  $R_2 = \infty$  and  $\alpha_2 = 0$ , indicating immunity to perturbations. Practically, we seek large  $R$  and small  $\alpha_2$  for robustness.

In essence, Definition 1 offers a holistic framework for FTS, encompassing forecast similarity, stability, and accuracy in time series forecasting.

**Definition 2 ( $\mu$ -Rényi divergence).** *Given two probability distributions  $P$  and  $Q$ , and  $\alpha \in (1, \infty)$ , the  $\mu$ -Rényi divergence  $D_\mu(P||Q)$  is defined as  $D_\mu(P||Q) = \frac{1}{\mu-1} \log \mathbb{E}_{x \sim Q} \left( \frac{P(x)}{Q(x)} \right)^\mu$ .*

Rényi divergence [45] is a generalization of the traditional Kullback-Leibler divergence that can be controlled with a parameter  $\mu$ . It measures the difference between probability distributions. When  $\mu \rightarrow 0$ , Rényi divergence tends towards Kullback-Leibler divergence, and when  $\mu = 0$  or  $\mu = \infty$ , Rényi divergence becomes the minimum and maximum divergence, respectively.

The next two theorems will state properties in IB Space, namely Similarity in IB Space. Theorem 1 begins with a rough estimate of the similarity from which we can estimate an upper bound on the fluctuations in IB Space for any IB Space and any input. Theorem 2 derives a lower bound on the fluctuations in IB Space in the condition is satisfied, it can be shown that our model is stable.

**Theorem 1 (Upper bound for sib ).** *If function  $f(\cdot)$  is a decoder function, which is considered under  $(\alpha_1, \alpha_2, \beta, \delta, R_1, R_2, \|\cdot\|)$ -Faithful TimeSieve, then if*

$$\beta \leq \|\hat{\pi}_i(x(t)) - \hat{\pi}_i(x(t) + \delta)\| ,$$

where  $i \in [a, d]$ , we have for all  $x(t)' \triangleq x(t) + \delta$  such that where  $\|x(t) - x(t)'\| \leq R_1$ ,

$$\|f(z, \hat{\pi}_i; \theta_d) - f(z, \hat{\pi}_i'; \theta_d)\| \leq c\delta ,$$

where  $\hat{\pi}_i' \triangleq \hat{\pi}_i(x(t) + \delta)$  and  $c$  is a constant. The proof of Theorem 1 shows in Appendix A.

**Theorem 2 (Lower bound for sib ).** *If function  $f(\cdot)$  is a decoder function, which is considered under  $(\alpha_1, \alpha_2, \beta, \delta, R_1, R_2, \|\cdot\|)$ -Faithful TimeSieve and IB Space expanded by measurements  $D_\mu, \|\cdot\|$ . Then if  $\delta \sim \mathcal{N}(0, \sigma^2)$ , for any  $\mu \in (1, \infty)$  and input  $x(t)$  we have*

$$\sigma^2 \geq \max \left\{ \delta, \frac{\mu R_1^2}{2\beta} \right\} .$$

The proof of Theorem 2 shows in Appendix B. Theorem 2 indicates that similarity exists in IB Space for input  $x(t)$  when  $\sigma^2$  is large enough.

Equivalently, based Theorem 1 and 2 we can also get the bound for CPS and SNP, we give these two properties without proof in Appendix.

**Theorem 3 (Consistency in prediction space).** *If function  $y(\cdot)$  is the function of the model, which is considered under  $(\alpha_1, \alpha_2, \beta, \delta, R_1, R_2, \|\cdot\|)$ -Faithful TimeSieve, we have*

$$D_2(y(x(t), \tilde{\omega}) - y(x(t), \omega)) \leq c\delta = \alpha_1 ,$$

where  $c$  is a constant and  $D_2$  could be a norm  $\|\cdot\|$ .

**Definition 3 (Stable Diameter).** *In FTS, if  $R_1$  and  $\alpha_1$  are bounded, the **Stable Diameter**  $R_2$  is defined as*

$$R_2 = \sup_{R \in \mathcal{R}} R \leq R_1, \text{ s.t. } D_2(y(x(t), \tilde{\omega}) - y(x(t), \omega)) \leq \alpha_1 ,$$

where  $\mathcal{R}$  is the set of all potential diameters.

Our FTS framework ensures SNP under the stable diameter as defined in Definition 3, supported by Theorem 4.

**Theorem 4 (Stability in noise perturbations).** *If function  $y(\cdot)$  is the function of FTS model, which is considered under  $(\alpha_1, \alpha_2, \beta, \delta, R_1, R_2, \|\cdot\|)$ -Faithful TimeSieve expanded by measurements  $D_\mu, \|\cdot\|$ . Then for all  $R$  in set  $\mathcal{R}$ , we have*

$$D_3(y(x(t), \tilde{\omega}), y(x(t) + \delta, \tilde{\omega})) \leq \alpha_2, \text{ s.t. } \|\delta\| \leq R_2 ,$$

where  $D_3$  could be a norm  $\|\cdot\|$ , and  $\alpha_2 \leq \alpha_1$ , which is decided by stable diameter.

### 3.5 Faithful TimeSieve Framework

We have already presented a rigorous definition of FTS. To construct FTS, we formulate a minimax optimization problem incorporating three conditions as outlined in Definition 1. The definition enables us to establish an initial optimization problem, from which we derive the following comprehensive objective function (the framework is shown in Figure 2):

$$\begin{aligned}
 & \max_{\|\delta\| \leq R} \lambda_1 (\beta - D_1(\hat{\pi}_a(x(t)), \hat{\pi}_a(x(t) + \delta))) \\
 & + \max_{\|\delta\| \leq R} \lambda_1 (\beta - D_1(\hat{\pi}_d(x(t)), \hat{\pi}_d(x(t) + \delta))) \\
 & + \min_{\tilde{\omega}} \mathbb{E}_x [\lambda_2 (D_2(y(x(t), \tilde{\omega}), y(x(t), \omega)) - \alpha_1)] \\
 & + \max_{\|\delta\| \leq R} \lambda_3 (D_3(y(x(t), \tilde{\omega}), y(x(t) + \delta, \tilde{\omega})) - \alpha_2).
 \end{aligned} \tag{7}$$

The min-max optimization problem discussed involves hyperparameters  $\lambda_i$ , where  $i \in [3]$ .

Inspired by the Projected Gradient Descent (PGD) methodology proposed by Madry et al. [46], the optimization process involves iterative updates to  $\delta$  and  $\rho$ . At the  $p$ -th iteration for updating the current noise  $\delta_{p-1}^*$ , we perform the following steps:

$$\begin{aligned}
 \delta_p &= \delta_{p-1}^* + \frac{\gamma_p}{|A_{p-1}|} \sum_{x \in A_{p-1}} \nabla_{\delta_{p-1}^*} \\
 & [D_1(\hat{\pi}_a(x(t)), \hat{\pi}_a(x(t) + \delta_{p-1}^*)) + D_2(y(x(t), \tilde{\omega}), y(x(t), \omega)) \\
 & + D_3(y(x(t), \tilde{\omega}), y(x(t) + \delta_{p-1}^*, \tilde{\omega}))],
 \end{aligned} \tag{8}$$

where  $\delta_p^* = \arg \min_{\|\delta\| \leq R} \|\delta - \delta_p\|$  and  $A_{p-1}$  denotes a batch of samples,  $\gamma_p$  is the step size parameter for PGD, and  $R$  is the norm bound for the perturbation.

Once  $\delta_P$  is obtained after  $P$  iterations, we update  $\tilde{\omega}^{t-1}$  to  $\tilde{\omega}^t$  using batched gradients.

Finally, we have the following objective function:

$$\begin{aligned}
 & \min_{\tilde{\omega}} \mathbb{E}_x [\lambda_1 \underbrace{(D_1(\hat{\pi}_i(x(t)), \hat{\pi}_i(x(t) + \delta))}_{\mathcal{L}_{sib, i \in [a, d]}}) \\
 & + \lambda_2 \underbrace{D_2(y(x(t), \tilde{\omega}), y(x(t), \omega))}_{\mathcal{L}_{cps}} \\
 & + \lambda_3 \underbrace{D_3(y(x(t), \tilde{\omega}), y(x(t) + \delta, \tilde{\omega}))}_{\mathcal{L}_{snp}}].
 \end{aligned} \tag{9}$$

We incorporate the three mentioned losses as auxiliary attention stability losses into the original TS model loss  $\mathcal{L} = \mathcal{L}_{reg} + \mathcal{L}_{IB}$  for fine-tuning. Eventually, we obtain:

$$\mathcal{L} = \mathcal{L}_{reg} + \mathcal{L}_{IB} + \lambda_1 \cdot \mathcal{L}_{sib} + \lambda_2 \cdot \mathcal{L}_{cps} + \lambda_3 \cdot \mathcal{L}_{snp}, \tag{10}$$

where  $\lambda_1$ ,  $\lambda_2$  and  $\lambda_3$  are regularizations of each loss function. The pseudocode for the faithful TimeSieve framework – Algorithm 1 is shown in Appendix C.

## 4 Experiments and Results

### 4.1 Settings

**Dataset.** We conduct extensive experiments to evaluate the efficacy of FTS. When it comes to multivariate forecasting, we employ a range of real-world benchmarks, such as ETT [18] and Exchange [47]. Notably, rather than employing a fixed lookback window length, we adopt the strategy introduced by Koopa [48] where the lookback window length  $T$  is

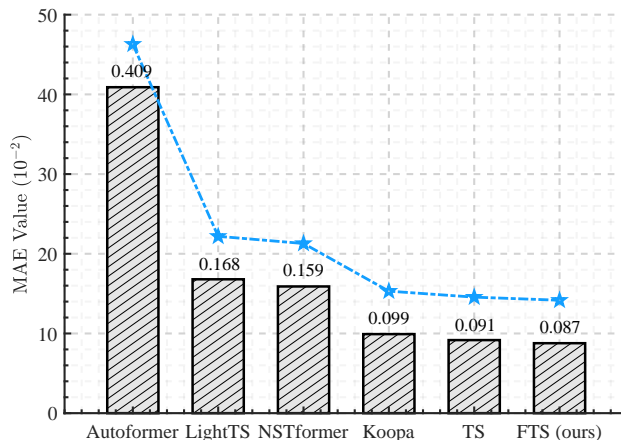


Figure 3: This figure displays a performance comparison of various advanced models under conditions without any added perturbations, with performance ranked from best to worst from left to right. The left ordinate and the bold values on the bars represent the MAE loss of each model, while the right ordinate and the labeled values indicate the percentage of performance improvement over the Autoformer.

set to twice the forecast window length (i.e.,  $T = 2H$ ). This methodology is grounded in the accessibility of historical data in practical scenarios, where leveraging a larger volume of observed data can significantly improve the model’s performance, particularly for longer forecasts.

**Random seeds.** In the context of our random seeds experiments, we deliberately varied the initial random seed values to assess the impact on model training and subsequent performance. Specifically, we opted for a set of ten distinct seeds: 2021, 2022, 2023, 2024, 2025, 2026, 2027, 2028, 2029 and 2030 and use 2021 be the based random seed. By utilizing these different seeds, we aimed to investigate the sensitivity of the trained models to variations in the random initialization process.

**Input perturbations and intermediate layer perturbations.** Our proposed framework demonstrated certain faithfulness against input perturbations and intermediate layer perturbations. To prove this, we designed and conducted comparative experiments. In these experiments, we introduced a type of noise more suited to time series forecasting tasks. This noise is generated through sequence decomposition [15], and we selected the residual part as the noise source [16]. By introducing this noise, we are able to simulate disturbances commonly encountered in real-world time series tasks, thereby assessing the model’s capability to handle specific disruptions in time series data. To further prove the model’s robustness, we opted to directly add Gaussian noise to the parameters of the model’s critical layer (IFCB layer). Specifically, we target the input of model and the parameters of the IFCB layer and then embed noise directly into these input ( $x(t)' = x(t) + \mathcal{N}(0, \sigma)$ , with a perturbation of a certain radius  $\sigma$ ) and parameters ( $\theta'_{IFCB} = \theta_{IFCB} + \mathcal{N}(0, \sigma)$ ). This approach allows for a more direct assessment of the model’s performance in the face of key parameter perturbations. More introduction you can see in Appendix F.

**Setup.** The hardware utilized for our experiments comprised an NVIDIA GeForce RTX 3090 GPU and an Intel(R) Xeon(R) E5-2686 v4 CPU, ensuring the computational efficiency required for intensive model training and evaluation. We trained our models over 10 epochs with a batch size of 32 and a learning rate of 0.0001 to optimize convergence without overfitting.

## 4.2 Performance under No Perturbations

We first compare FTS with other advanced models (TS [7], Koopa [12], Non-stationary Transformers (NSTformer) [4], LightTS [13], Autoformer [15]), and the results are shown in Figure 3.

It can be seen that even with only faithful optimization, the performance on the original dataset without added noise is still superior to that of the unoptimized model. We are surprised to find that our framework not only did not perform worse in the original case without additional perturbations, but instead managed to achieve a higher performance (SOTA). The explanation for our preliminary analysis is that the data for timing problems inherently has perturbations, and our method effectively improves the generalization of the model, making it perform better on the original task.



Table 1: A performance comparison of FTS and TS on the Exchange dataset, with a prediction length of 96 steps, using MSE as the metric. The results reveal that FTS consistently outperforms TS and is less susceptible to the selection of random seeds. The baseline values used in the calculation correspond to the 2021 random seed performance. The 'Preference' percentage, a metric of performance advantage, is calculated using the following formula: Preference (%) =  $\left(1 - \frac{|V_{fts_b} - V_{fts_c}|}{|V_{ts_b} - V_{ts_c}|} \times \frac{V_{ts_b}}{V_{fts_b}}\right) \times 100\%$ . Here,  $V_{fts_b}$  and  $V_{ts_b}$  represent the MSE values for the FTS and TS models, respectively, under the 2021 random seed (based one), while  $V_{fts_c}$  and  $V_{ts_c}$  are the values under the current random seed being analyzed.

Random seed	TS	FTS	Preference(%)
2021*	0.0929	0.0868	NA
2022	0.0989	0.0867	<b>99.61%</b>
2023	0.0819	0.0864	<b>96.09%</b>
2024	0.0993	0.0860	<b>87.95%</b>
2025	0.0917	0.0878	<b>4.49%</b>
2026	0.0960	0.0876	<b>69.27%</b>
2027	0.0826	0.0892	<b>74.16%</b>
2028	0.0818	0.0863	<b>95.81%</b>
2029	0.1160	0.0879	<b>94.69%</b>
2030	0.0897	0.0898	<b>1.53%</b>

### 4.3 Faithfulness under Different Random Seeds

To demonstrate the stability of our model’s performance across various random seeds, we conducted a comparative analysis of the performances of FTS and TS under multiple seed settings, with detailed results presented in Table 1 in Exchange dataset. We specifically chose the performance metrics from the 2021 seed’s model as our based model, which allowed us to quantitatively assess how FTS diminishes the variability induced by different seeds compared to TS. This analysis revealed that FTS consistently reduced the influence of seed variability on performance metrics, with a significant reduction of up to 99.61%. Details on the specific calculation method for this reduction can be found in the appendix D.

We selected the performance under the random seed 2021 as our base model and calculated the reduction in seed variability by FTS compared to TS. Figures 1 clearly illustrate that FTS maintains more consistent performance than TS.

### 4.4 Faithfulness under Input and Parameter Perturbations

Table 2: Experimental results demonstrating the robustness of the proposed model under various perturbation conditions. The table compares the MAE and MSE of the model under different perturbation scenarios: No Perturbation (NP), No Perturbation with Optimization (NPO), Input Perturbation (IP), Input Perturbation with Optimization (IPO), Intermediate Layer Perturbation (ILP), and Intermediate Layer Perturbation with Optimization (ILPO).

Conditions	Metric	NP		NPO		IP		IPO		ILP		ILPO	
		MAE	MSE	MAE	MSE	MAE	MSE	MAE	MSE	MAE	MSE	MAE	MSE
ETTh1	48	0.361	0.341	0.360 ↓ <sub>0.001</sub>	0.341	0.386	0.375	0.376 ↓ <sub>0.010</sub>	0.361 ↓ <sub>0.014</sub>	0.437	0.456	0.392 ↓ <sub>0.045</sub>	0.392 ↓ <sub>0.064</sub>
	96	0.384	0.377	0.384	0.376 ↓ <sub>0.001</sub>	0.411	0.424	0.404 ↓ <sub>0.007</sub>	0.408 ↓ <sub>0.016</sub>	0.415	0.422	0.401 ↓ <sub>0.014</sub>	0.397 ↓ <sub>0.025</sub>
	144	0.397	0.393	0.396 ↓ <sub>0.001</sub>	0.393	0.422	0.437	0.413 ↓ <sub>0.009</sub>	0.422 ↓ <sub>0.015</sub>	0.483	0.520	0.447 ↓ <sub>0.036</sub>	0.472 ↓ <sub>0.048</sub>
	192	0.408	0.404	0.406 ↓ <sub>0.002</sub>	0.402 ↓ <sub>0.002</sub>	0.431	0.445	0.420 ↓ <sub>0.011</sub>	0.426 ↓ <sub>0.019</sub>	0.443	0.451	0.428 ↓ <sub>0.015</sub>	0.430 ↓ <sub>0.021</sub>
Exchange	48	0.140	0.043	0.139 ↓ <sub>0.001</sub>	0.042 ↓ <sub>0.001</sub>	0.220	0.102	0.186 ↓ <sub>0.034</sub>	0.073 ↓ <sub>0.029</sub>	0.160	0.045	0.148 ↓ <sub>0.012</sub>	0.044 ↓ <sub>0.001</sub>
	96	0.197	0.086	0.198	0.087	0.265	0.131	0.237 ↓ <sub>0.028</sub>	0.104 ↓ <sub>0.027</sub>	0.221	0.102	0.202 ↓ <sub>0.019</sub>	0.092 ↓ <sub>0.010</sub>
	144	0.243	0.124	0.242 ↓ <sub>0.001</sub>	0.123 ↓ <sub>0.001</sub>	0.312	0.175	0.271 ↓ <sub>0.041</sub>	0.141 ↓ <sub>0.034</sub>	0.292	0.164	0.253 ↓ <sub>0.039</sub>	0.149 ↓ <sub>0.015</sub>
	192	0.292	0.179	0.287 ↓ <sub>0.005</sub>	0.170 ↓ <sub>0.009</sub>	0.345	0.239	0.307 ↓ <sub>0.038</sub>	0.178 ↓ <sub>0.061</sub>	0.331	0.205	0.304 ↓ <sub>0.027</sub>	0.190 ↓ <sub>0.015</sub>

To demonstrate the effectiveness of the proposed framework, we evaluated its faithfulness under different perturbation conditions in this experiment, as shown in Table 2. The table lists the model’s performance under no perturbation, input perturbation, and intermediate layer perturbation, both before and after optimization. The experimental results are measured using two metrics: Mean Absolute Error (MAE) and Mean Squared Error (MSE). We conducted experiments on two datasets: ETTh1 and Exchange, with prediction lengths of 48, 96, 144, and 192 steps.

**No perturbation and no perturbation with optimization.** Under no perturbation conditions (NP), the baseline performance of the model is shown. By comparing the results of no perturbation with optimization (NPO), we can see that the optimized model shows slight improvement in most cases. This is consistent with our previous conclusion that time series data inherently contains perturbations, and our method effectively enhances the model’s generalization ability, thereby improving its performance on the original task. For example, in the Exchange dataset, the MAE for 192 steps prediction decreased from 0.292 to 0.287 and the MSE for 192 steps prediction decreased from 0.179 to 0.170.

**Input perturbation and input perturbation with optimization.** Under input perturbation conditions (IP), the model’s performance declines to some extent, indicating that input noise indeed affects the model’s prediction accuracy. In the ETTh1 dataset, the MAE for 96 steps prediction increased from 0.384 to 0.411, while in the Exchange dataset, the MAE for 48 steps prediction increased from 0.140 to 0.220. However, through input perturbation with optimization (IPO), the model’s performance significantly improved. For instance, in the ETTh1 dataset, the MAE for 144 steps prediction decreased from 0.422 to 0.413, a 36% reduction in perturbation. In the Exchange dataset, the MAE for 48 steps prediction decreased from 0.220 to 0.186, a 42.5% reduction in perturbation. This demonstrates that PGD attacks can effectively identify the weak parts of the input data, and through optimization, these weak parts are strengthened, thereby enhancing the model’s robustness and faithfulness. Details on the experiments with different types of noise for input perturbations, as well as the PGD parameter settings for input perturbations, can be found in Appendix E.1 and Appendix E.3.

**Intermediate layer perturbation and intermediate layer perturbation with optimization.** Under intermediate layer perturbation conditions (ILP), the impact on the model’s performance is more significant, especially in the MSE metric, indicating that perturbations in the intermediate layer parameters have a greater effect on the model’s predictions. For example, in the ETTh1 dataset, the MSE for 144 steps prediction increased from 0.393 to 0.520, while in the Exchange dataset, the MSE for 192 steps prediction increased from 0.179 to 0.205. However, through intermediate layer perturbation with optimization (ILPO), the model’s performance also improved. In the ETTh1 dataset, the 192 steps prediction MSE dropped from 0.451 to 0.430, a 44.7% reduction. For the Exchange dataset, the 144 steps prediction MSE fell from 0.164 to 0.149, a 37.5% decrease. This shows that PGD attacks can optimize model weaknesses under intermediate layer perturbation, enhancing robustness. Further experiments on larger perturbations are detailed in Appendix E.2.

#### 4.5 Loss Function Ablation Study

Table 3: This table presents the results of the loss function ablation study, which evaluates the robustness of the proposed framework by combining different loss functions. The performance metrics used are MAE and MSE, measured across four prediction lengths: 48, 96, 144, and 192 steps. The datasets used are ETTh1 and Exchange.

Loss		$\mathcal{L}_{total}$		$\mathcal{L}_{no\_snp}$		$\mathcal{L}_{no\_cps}$		$\mathcal{L}_{no\_sib}$		$\mathcal{L}_{no\_cps+sib}$		$\mathcal{L}_{no\_snp+sib}$		$\mathcal{L}_{no\_snp+cps}$		$\mathcal{L}_{no\_snp+cps+sib}$	
Metric		MAE	MSE	MAE	MSE	MAE	MSE	MAE	MSE	MAE	MSE	MAE	MSE	MAE	MSE	MAE	MSE
ETTh1	48	<b>0.376</b>	<b>0.361</b>	0.383	0.370	0.381	0.363	0.378	<b>0.361</b>	0.381	0.365	0.383	0.370	0.384	0.372	0.382	0.371
	96	<b>0.404</b>	<b>0.408</b>	0.409	0.419	0.405	0.410	<b>0.404</b>	0.408	<b>0.404</b>	0.410	0.410	0.419	0.411	0.421	0.410	0.420
	144	<b>0.413</b>	<b>0.422</b>	0.423	0.431	<b>0.413</b>	0.423	0.417	<b>0.422</b>	0.414	<b>0.422</b>	0.423	0.431	0.423	0.430	0.420	0.429
	192	<b>0.420</b>	<b>0.426</b>	0.425	0.433	0.428	0.431	0.423	<b>0.426</b>	0.425	0.430	0.428	0.433	0.430	0.433	0.427	0.429
Exchange	48	<b>0.186</b>	<b>0.073</b>	0.195	0.078	0.190	0.084	0.191	0.074	0.190	0.085	0.195	0.078	0.197	0.083	0.195	0.080
	96	0.237	<b>0.104</b>	0.238	0.112	0.242	0.126	<b>0.235</b>	0.106	0.242	0.126	0.238	0.112	0.244	0.139	0.241	0.137
	144	0.271	0.141	0.277	0.150	0.281	0.177	<b>0.270</b>	<b>0.139</b>	0.281	0.178	0.278	0.150	0.280	0.192	0.280	0.188
	192	0.307	<b>0.178</b>	0.309	0.191	0.317	0.236	<b>0.305</b>	0.180	0.318	0.236	0.310	0.188	0.314	0.254	0.314	0.254

In these experiments, we evaluated the robustness and faithfulness of the proposed framework through different combinations of loss functions, as shown in Table 3. The experimental results are measured using also MAE and MSE and covered two datasets: ETTh1 and Exchange. We designed eight different loss function combinations:  $\mathcal{L}_{total}$ ,  $\mathcal{L}_{no\_snp}$ ,  $\mathcal{L}_{no\_cps}$ ,  $\mathcal{L}_{no\_sib}$ ,  $\mathcal{L}_{no\_cps+sib}$ ,  $\mathcal{L}_{no\_snp+sib}$ ,  $\mathcal{L}_{no\_snp+cps}$  and  $\mathcal{L}_{no\_snp+cps+sib}$  to explore the contribution of each loss function to the improvement of model faithfulness. Experiments detailing the parameter settings for the loss function parameters can be found in the Appendix E.4.

**$\mathcal{L}_{total}$  Combination.** In most prediction horizons, the  $\mathcal{L}_{total}$  combination showed the best MAE and MSE performance. For example, in the ETTh1 dataset for 48 steps prediction, the MAE is 0.376 and the MSE is 0.361; in the Exchange dataset for 48 steps prediction, the MAE is 0.186 and the MSE is 0.073. This indicates that the combination of all loss functions effectively improves the model’s prediction accuracy and robustness. The excellent performance on both datasets suggests that  $\mathcal{L}_{total}$  adapts well to datasets with different characteristics.

**$\mathcal{L}_{no\_snp}$  Combination.** Removing the  $\mathcal{L}_{snp}$  resulted in a performance decline on both datasets. For example, in the ETTh1 dataset for 48 steps prediction, the MAE increased to 0.383 and the MSE to 0.370; in the Exchange dataset for

48 steps prediction, the MAE increased to 0.195 and the MSE to 0.078. This shows that the  $\mathcal{L}_{snp}$  plays a crucial role in maintaining the consistency of the model’s output before and after input perturbations. It ensures that the model does not exhibit significant accuracy drops in its original task even after optimization. The ETTh1 and Exchange datasets exhibit different sensitivities to input perturbations. The ETTh1 dataset, common in industrial scenarios, may contain periodic and seasonal components that are sensitive to perturbations. The significant increase in prediction error after removing  $\mathcal{L}_{snp}$  reflects its high sensitivity to input perturbations. The Exchange dataset, reflecting currency Exchange rate changes between different countries, may include more random fluctuations and sudden changes. Although performance also declines after removing  $\mathcal{L}_{snp}$ , the drop is relatively smaller, indicating that the Exchange is more robust.

**$\mathcal{L}_{no\_cps}$  Combination.** After the removal of the  $\mathcal{L}_{cps}$ , there is a slight decrease in model performance on the ETTh1 dataset, such as an MAE of 0.381 and MSE of 0.363 for the 48 steps prediction. This indicates that the  $\mathcal{L}_{cps}$  is effective in certain scenarios, and maintaining constraints consistent with the original model output is beneficial for enhancing model robustness. Additionally, we observed a more significant performance decline on the Exchange dataset in the absence of the  $\mathcal{L}_{cps}$ . This may be because the Exchange dataset involves currency exchange rates between different countries, a type of data often subject to considerable random fluctuations and impacts from external economic events, resulting in more complex and unstable time series data. Constraints on the original model output may help the model maintain consistency and resist noise in this unstable environment. Once these constraints are removed, the model may struggle more with handling random fluctuations and extreme values in the data.

**$\mathcal{L}_{no\_sib}$  Combination.** Removing the  $\mathcal{L}_{sib}$  resulted in a performance decline on both datasets. For example, in the ETTh1 dataset for 48 steps prediction, the MAE is 0.378 and the MSE is 0.361; in the Exchange dataset for 48 steps prediction, the MAE is 0.191 and the MSE is 0.074. This indicates that the  $\mathcal{L}_{sib}$  plays an active role in enhancing the stability of intermediate layer features. The performance decline after removing  $\mathcal{L}_{sib}$  shows that the stability of intermediate layer features significantly impacts the model’s performance on datasets with different behavioral patterns. Additionally, we found that removing the IB critical layer similarity constraint resulted in a slight improvement in the Exchange dataset for 144 steps prediction, whereas ETTh1 did not exhibit a similar improvement. This may be due to the Exchange dataset containing more random fluctuations and sudden changes, allowing the model to more flexibly adapt to these variations after removing the constraint. In contrast, the periodic and trend characteristics of the ETTh1 dataset demand higher stability of intermediate layer features, and removing the constraint did not enhance performance.

**$\mathcal{L}_{no\_cps+sib}$  Combination.** The performance also declined after simultaneously removing the  $\mathcal{L}_{cps}$  and the  $\mathcal{L}_{sib}$ . However, it is relatively closer to the performance with just the  $\mathcal{L}_{cps}$  loss removed. For example, on the Exchange dataset for the 96 steps prediction, both  $\mathcal{L}_{no\_cps+sib}$  and  $\mathcal{L}_{no\_cps}$  had an MAE of 0.242. This suggests that relatively speaking, the  $\mathcal{L}_{cps}$  has a greater impact on the model compared to the  $\mathcal{L}_{sib}$ .

**$\mathcal{L}_{no\_snp+sib}$  Combination.** After the simultaneous removal of both  $\mathcal{L}_{snp}$  and  $\mathcal{L}_{sib}$  components, the model exhibited a decrement in performance. This decline is reminiscent of the effects observed when both  $\mathcal{L}_{cps}$  and  $\mathcal{L}_{sib}$  are absent, with the resultant performance more closely aligning with that observed in the absence of  $\mathcal{L}_{cps}$  alone. The results suggest that  $\mathcal{L}_{sib}$  has a less significant impact on model performance than  $\mathcal{L}_{cps}$ .

**$\mathcal{L}_{no\_snp+cps}$  Combination.** Upon elimination of both the loss terms  $\mathcal{L}_{snp}$  and  $\mathcal{L}_{cps}$ , the model’s performance suffers a decline when compared to the scenario where only one of these loss terms is removed. For instance, on the Exchange dataset with a 96 steps prediction,  $\mathcal{L}_{no\_snp+cps}$  records a value of 0.244, whereas  $\mathcal{L}_{no\_snp}$  and  $\mathcal{L}_{no\_cps}$  register 0.238 and 0.242, respectively. This observation suggests that the  $\mathcal{L}_{snp}$  and the  $\mathcal{L}_{cps}$  can indeed provide beneficial constraints on the model’s parameter updates under certain conditions, and facilitate optimal model training performance.

**$\mathcal{L}_{no\_snp+cps+sib}$  Combination.** We have observed that sometimes, removing three components of the loss function results in better performance than removing only two. For instance, in the Exchange dataset with a prediction horizon of 48 steps, the performance of  $\mathcal{L}_{no\_snp+cps+sib}$  surpasses that of  $\mathcal{L}_{no\_snp+cps}$ , with MAE values of 0.195 and 0.197 respectively. The complexity of the optimization process can increase with multiple loss functions, potentially leading to a more intricate loss landscape. This can cause a tug-of-war effect on model parameters, making it challenging to achieve a balanced solution. Thus, a more streamlined set of loss terms might lead to better performance.

## 5 Conclusions

This study underscores the importance of fidelity in time series forecasting models, particularly within the TS framework. We have identified and addressed the model’s high faithfulness to random seeds, input perturbations, and layer disturbances, highlighting the necessity for developing robust and faithful forecasting mechanisms. To this end, we introduced an innovative framework that enhances the fidelity of TimeSieve through a rigorous definition, effectively mitigating these vulnerabilities.

Our research provides faithful technical support and theoretical support to the field of time series forecasting, promising to advance the development and reliability of forecasting methods within the industry. Through these efforts, we aim to bolster the trustworthiness of models, ultimately supporting decision-making processes that rely on accurate and consistent predictions.

Looking forward, we aspire to make this framework can be applied to enhance the faithfulness of not just TimeSieve but also other state-of-the-art temporal methods, thereby contributing to the reliability and robustness of temporal modeling as a whole.

## References

- [1] Rahul Dey and Fathi M. Salem. Gate-variants of gated recurrent unit (gru) neural networks. In *2017 IEEE 60th International Midwest Symposium on Circuits and Systems (MWSCAS)*, pages 1597–1600, 2017.
- [2] Klaus Greff, Rupesh K Srivastava, Jan Koutník, Bas R Steunebrink, and Jürgen Schmidhuber. Lstm: A search space odyssey. *IEEE transactions on neural networks and learning systems*, 28(10):2222–2232, 2016.
- [3] Yuqi Nie, Nam H. Nguyen, Phanwadee Sinthong, and Jayant Kalagnanam. A time series is worth 64 words: Long-term forecasting with transformers, 2023.
- [4] Yong Liu, Haixu Wu, Jianmin Wang, and Mingsheng Long. Non-stationary transformers: Exploring the stationarity in time series forecasting, 2023.
- [5] Haixu Wu, Tengge Hu, Yong Liu, Hang Zhou, Jianmin Wang, and Mingsheng Long. Timesnet: Temporal 2d-variation modeling for general time series analysis, 2023.
- [6] Kun Yi, Qi Zhang, Wei Fan, Shoujin Wang, Pengyang Wang, Hui He, Defu Lian, Ning An, Longbing Cao, and Zhendong Niu. Frequency-domain mlps are more effective learners in time series forecasting, 2023.
- [7] Ninghui Feng, Songning Lai, Fobao Zhou, Zhenxiao Yin, and Hang Zhao. Timesieve: Extracting temporal dynamics through information bottlenecks, 2024.
- [8] Dengsheng Zhang and Dengsheng Zhang. Wavelet transform. *Fundamentals of image data mining: Analysis, Features, Classification and Retrieval*, pages 35–44, 2019.
- [9] Ram Shankar Pathak. *The wavelet transform*, volume 4. Springer Science & Business Media, 2009.
- [10] Paul M Bentley and JTE McDonnell. Wavelet transforms: an introduction. *Electronics & communication engineering journal*, 6(4):175–186, 1994.
- [11] Ravid Shwartz-Ziv and Naftali Tishby. Opening the black box of deep neural networks via information. *arXiv preprint arXiv:1703.00810*, 2017.
- [12] Yong Liu, Chenyu Li, Jianmin Wang, and Mingsheng Long. Koopa: Learning non-stationary time series dynamics with koopman predictors. *Advances in Neural Information Processing Systems*, 36, 2024.
- [13] David Campos, Miao Zhang, Bin Yang, Tung Kieu, Chenjuan Guo, and Christian S Jensen. Lightts: Lightweight time series classification with adaptive ensemble distillation. *Proceedings of the ACM on Management of Data*, 1(2):1–27, 2023.
- [14] Yong Liu, Haixu Wu, Jianmin Wang, and Mingsheng Long. Non-stationary transformers: Exploring the stationarity in time series forecasting. *Advances in Neural Information Processing Systems*, 35:9881–9893, 2022.
- [15] Haixu Wu, Jiehui Xu, Jianmin Wang, and Mingsheng Long. Autoformer: Decomposition transformers with auto-correlation for long-term series forecasting. *Advances in neural information processing systems*, 34:22419–22430, 2021.
- [16] Shuhan Zhong, Sizhe Song, Weipeng Zhuo, Guanyao Li, Yang Liu, and S. H. Gary Chan. A multi-scale decomposition mlp-mixer for time series analysis, 2024.
- [17] Ailing Zeng, Muxi Chen, Lei Zhang, and Qiang Xu. Are transformers effective for time series forecasting?, 2022.
- [18] Haoyi Zhou, Shanghang Zhang, Jieqi Peng, Shuai Zhang, Jianxin Li, Hui Xiong, and Wancai Zhang. Informer: Beyond efficient transformer for long sequence time-series forecasting, 2021.
- [19] R Douglas Martin. Robust methods for time series. In *Applied time series analysis II*, pages 683–759. Elsevier, 1981.
- [20] Jurgen Franke. On the robust prediction and interpolation of time series in the presence of correlated noise. *Journal of Time Series Analysis*, 5(4):227–244, 1984.

- [21] Songning Lai, Ninghui Feng, Haochen Sui, Ze Ma, Hao Wang, Zichen Song, Hang Zhao, and Yutao Yue. Fts: A framework to find a faithful timesieve. *arXiv preprint arXiv:2405.19647*, 2024.
- [22] Yitong Li, Kai Wu, and Jing Liu. Self-paced arima for robust time series prediction. *Knowledge-Based Systems*, 269:110489, 2023.
- [23] Zongdong Liu and Jing Liu. A robust time series prediction method based on empirical mode decomposition and high-order fuzzy cognitive maps. *Knowledge-Based Systems*, 203:106105, 2020.
- [24] Hiroshi Okamura, Yutaka Osada, Shota Nishijima, and Shinto Eguchi. Novel robust time series analysis for long-term and short-term prediction. *Scientific Reports*, 11(1):11938, 2021.
- [25] Shoubo Feng, Weijie Ren, Min Han, and Yen Wei Chen. Robust manifold broad learning system for large-scale noisy chaotic time series prediction: A perturbation perspective. *Neural networks*, 117:179–190, 2019.
- [26] Zijian Zeng and Meng Li. Bayesian median autoregression for robust time series forecasting. *International Journal of Forecasting*, 37(2):1000–1010, 2021.
- [27] Zhiqiang Zhou, Linxiao Yang, Qingsong Wen, and Liang Sun. Robusttsvar: A robust time series variance estimation algorithm. In *ICASSP 2024-2024 IEEE International Conference on Acoustics, Speech and Signal Processing (ICASSP)*, pages 161–165. IEEE, 2024.
- [28] Qingsong Wen, Kai He, Liang Sun, Yingying Zhang, Min Ke, and Huan Xu. Robustperiod: Robust time-frequency mining for multiple periodicity detection. In *Proceedings of the 2021 international conference on management of data*, pages 2328–2337, 2021.
- [29] TaeHo Yoon, Youngsuk Park, Ernest K Ryu, and Yuyang Wang. Robust probabilistic time series forecasting. In *International Conference on Artificial Intelligence and Statistics*, pages 1336–1358. PMLR, 2022.
- [30] Matteo Sangiorgio and Fabio Dercole. Robustness of lstm neural networks for multi-step forecasting of chaotic time series. *Chaos, Solitons & Fractals*, 139:110045, 2020.
- [31] Tian Guo, Zhao Xu, Xin Yao, Haifeng Chen, Karl Aberer, and Koichi Funaya. Robust online time series prediction with recurrent neural networks. In *2016 IEEE international conference on data science and advanced analytics (DSAA)*, pages 816–825. Ieee, 2016.
- [32] Sascha Krstanovic and Heiko Paulheim. Ensembles of recurrent neural networks for robust time series forecasting. In *Artificial Intelligence XXXIV: 37th SGAI International Conference on Artificial Intelligence, AI 2017, Cambridge, UK, December 12-14, 2017, Proceedings 37*, pages 34–46. Springer, 2017.
- [33] Dymitr Ruta. Crosstrained ensemble of neural networks for robust time series prediction. In *Proceedings of the NiSIS Symposium*, 2006.
- [34] Wenjuan Mei, Zhen Liu, and Yuanzhang Su. Mrpm: multistep robust prediction machine for degradation time series projection. In *2021 IEEE International Instrumentation and Measurement Technology Conference (I2MTC)*, pages 1–7. IEEE, 2021.
- [35] Jingkun Gao, Xiaomin Song, Qingsong Wen, Pichao Wang, Liang Sun, and Huan Xu. Robusttad: Robust time series anomaly detection via decomposition and convolutional neural networks. *arXiv preprint arXiv:2002.09545*, 2020.
- [36] Anguo Zhang, Wei Zhu, and Juanyu Li. Spiking echo state convolutional neural network for robust time series classification. *IEEE Access*, 7:4927–4935, 2018.
- [37] Guancheng Zhou. Robust time series prediction with missing data based on deep convolutional neural networks. In *2020 International Conference on Computer Communication and Network Security (CCNS)*, pages 178–183. IEEE, 2020.
- [38] Yunyao Cheng, Peng Chen, Chenjuan Guo, Kai Zhao, Qingsong Wen, Bin Yang, and Christian S Jensen. Weakly guided adaptation for robust time series forecasting. *Proceedings of the VLDB Endowment*, 17(4):766–779, 2023.
- [39] Xueli Zhang, Cankun Zhong, Jianjun Zhang, Ting Wang, and Wing WY Ng. Robust recurrent neural networks for time series forecasting. *Neurocomputing*, 526:143–157, 2023.
- [40] Owen Queen, Tom Hartvigsen, Teddy Koker, Huan He, Theodoros Tsiligkaridis, and Marinka Zitnik. Encoding time-series explanations through self-supervised model behavior consistency. *Advances in Neural Information Processing Systems*, 36, 2024.
- [41] Yang Yu, Ruizhe Ma, and Zongmin Ma. Robformer: A robust decomposition transformer for long-term time series forecasting. *Pattern Recognition*, page 110552, 2024.
- [42] Songning Lai, Lijie Hu, Junxiao Wang, Laure Berti-Equille, and Di Wang. Faithful vision-language interpretation via concept bottleneck models. In *The Twelfth International Conference on Learning Representations*, 2023.

- [43] Lijie Hu, Yixin Liu, Ninghao Liu, Mengdi Huai, Lichao Sun, and Di Wang. Seat: stable and explainable attention. In *Proceedings of the AAAI Conference on Artificial Intelligence*, volume 37, pages 12907–12915, 2023.
- [44] Wenshuo Chen, Hongru Xiao, Erhang Zhang, Lijie Hu, Lei Wang, Mengyuan Liu, and Chen Chen. Sato: Stable text-to-motion framework. *arXiv preprint arXiv:2405.01461*, 2024.
- [45] Tim Van Erven and Peter Harremoos. Rényi divergence and kullback-leibler divergence. *IEEE Transactions on Information Theory*, 60(7):3797–3820, 2014.
- [46] Aleksander Madry, Aleksandar Makelov, Ludwig Schmidt, Dimitris Tsipras, and Adrian Vladu. Towards deep learning models resistant to adversarial attacks. In *International Conference on Learning Representations*, 2018.
- [47] Guokun Lai, Wei-Cheng Chang, Yiming Yang, and Hanxiao Liu. Modeling long-and short-term temporal patterns with deep neural networks. In *The 41st international ACM SIGIR conference on research & development in information retrieval*, pages 95–104, 2018.
- [48] Yong Liu, Chenyu Li, Jianmin Wang, and Mingsheng Long. Koopa: Learning non-stationary time series dynamics with koopman predictors, 2023.

## A Proof for Theorem 1

*Proof.* In Section 3.1 we first define the approximation coefficients  $\pi_a$  and detail coefficients  $\pi_d$  as equation 1, representing the low-frequency trends and the high-frequency, respectively. For derivation convenience, we omit their arguments  $t$ , i.e.

$$\pi_i' = \pi_i(x(t) + \delta) = \int_{-\infty}^{\infty} (x(t) + \delta)\phi(t)dt$$

For all  $\delta \leq R_1$ , we have

$$\begin{aligned} \|\pi_a - \pi_a'\| &= \int_{-\infty}^{\infty} x(t)\phi(t)dt - \int_{-\infty}^{\infty} (x(t) + \delta)\phi(t)dt \\ &= \int_{-\infty}^{\infty} x(t)\phi(t)dt - \int_{-\infty}^{\infty} x(t)\phi(t)dt + \int_{-\infty}^{\infty} \delta\phi(t)dt \\ &= \int_{-\infty}^{\infty} \delta\phi(t)dt \end{aligned}$$

Claim:

$$\int_{-\infty}^{\infty} \delta\phi(t)dt \leq \delta$$

Due to the normalization of the scaling function, we have

$$\int_{-\infty}^{\infty} \phi(t)dt \equiv 1$$

Thus, the claim is established. There will be a same proof process in  $\pi_d$ . □

## B Proof for Theorem 2

*Proof.* Rényi divergence between two Gaussian distributions  $\mathcal{N}(0, \sigma^2\mathcal{I}_d)$  and  $\mathcal{N}(\delta, \sigma^2\mathcal{I}_d)$  is bounded by  $\frac{\mu\|\delta\|^2}{2\sigma^2}$ . Then we have

$$\begin{aligned} D_\mu(\hat{\pi}_i(x(t)), \hat{\pi}_i(x(t) + \delta)) &= D_\mu(f_i(z, x(t); \theta_d), f_i(z, x(t) + \delta; \theta_d)) \\ &\leq \frac{\mu\|x(t) - x(t) + \delta\|^2}{2\sigma^2} \leq \frac{\mu R_1^2}{2\sigma^2}. \end{aligned}$$

Thus, when  $\frac{\alpha R_1^2}{2\sigma^2} \leq \beta$ , the FTS framework will satisfy Similarity in IB Space. □

## C Pseudocode for FTS

The pseudocode for the faithful TimeSieve framework is shown in Algorithm 1.

---

**Algorithm 1:** Faithful TimeSieve
 

---

**input** : Weight matrix  $\omega$  of TimeSieve; Training data set  $D$ ; Training data input  $x(t)$ ; parameters  $\alpha_1, \alpha_2, \beta, R_1, R_2, \lambda_1, \lambda_2, \lambda_3$ . Iterations number  $T, P$ .

**output** :  $\tilde{\omega}^*$

1 **for**  $t = 1, 2, \dots, T$  **do**

2     Initialize  $\delta_0^*$  and  $\rho_0^*$ ;

3     **for**  $p = 1, 2, \dots, P$  **do**

4

$$\begin{aligned} \delta_p &= \delta_{p-1}^* + \frac{\gamma_p}{|A_{p-1}|} \sum_{x \in A_{p-1}} \nabla_{\delta_{p-1}^*} \\ &[D_1(\hat{\pi}_a(x(t)), \hat{\pi}_a(x(t) + \delta_{p-1}^*)) \\ &+ D_2(y(x(t), \tilde{\omega}), y(x(t), \omega)) \\ &+ D_3(y(x(t), \tilde{\omega}), y(x(t) + \delta_{p-1}^*, \tilde{\omega}))], \\ \delta_p^* &= \arg \min_{\|\delta\| \leq R} \|\delta - \delta_p\|. \end{aligned}$$

5     **end**

6     Randomly sample a batch  $C_t \subset D$ . **Update**  $\tilde{\omega}$ .

$$\begin{aligned} \tilde{\omega}^t &= \omega^{t-1} - \eta_t \sum_{x(t) \in C_t} [\nabla_{\tilde{\omega}} (\mathcal{L}_{\text{reg}} \\ &+ \mathcal{L}_{\text{IB}}) + \lambda_1 \underbrace{(D_1(\hat{\pi}_i(x(t)), \hat{\pi}_i(x(t) + \delta)))}_{\mathcal{L}_{\text{si}, i \in [a, d]}} \\ &+ \lambda_2 \nabla_{\tilde{\omega}} \underbrace{D_2(y(x(t), \tilde{\omega}), y(x(t), \omega))}_{\mathcal{L}_{\text{cps}}} \\ &+ \lambda_3 \nabla_{\tilde{\omega}} \underbrace{D_3(y(x(t), \tilde{\omega}), y(x(t) + \delta, \tilde{\omega}))}_{\mathcal{L}_{\text{snp}}}]_{\tilde{\omega}_c = \omega^{t-1}}]. \end{aligned}$$

7 **end**

8 **Return:**  $\tilde{\omega}^* = \tilde{\omega}_T$

---

## D Derivation of Preference Formula

In this appendix, we briefly derive the preference percentage formula used in our performance comparison table (Table 1). The preference percentage is calculated as follows:

$$\text{Preference (\%)} = \left( 1 - \frac{|V_{\text{ftsb}} - V_{\text{ftsc}}|}{|V_{\text{tsb}} - V_{\text{tsc}}|} \times \frac{V_{\text{tsb}}}{V_{\text{ftsb}}} \right) \times 100\%$$

First, calculate the MSE change for both FTS and TS models:

$$\Delta V_{\text{fts}} = |V_{\text{ftsb}} - V_{\text{ftsc}}|$$

$$\Delta V_{\text{ts}} = |V_{\text{tsb}} - V_{\text{tsc}}|$$

Next, compare these changes:

$$\frac{\Delta V_{\text{fts}}}{\Delta V_{\text{ts}}}$$

Adjust the ratio to account for baseline performance:

$$\frac{\Delta V_{fts}}{\Delta V_{ts}} \times \frac{V_{tsb}}{V_{ftsb}}$$

Finally, calculate the preference percentage:

$$\text{Preference (\%)} = \left( 1 - \left( \frac{\Delta V_{fts}}{\Delta V_{ts}} \times \frac{V_{tsb}}{V_{ftsb}} \right) \right) \times 100\%$$

where:

- $V_{ftsb}$ : MSE value for the FTS model under the baseline random seed (2021).
- $V_{tsb}$ : MSE value for the TS model under the baseline random seed (2021).
- $V_{ftsc}$ : MSE value for the FTS model under the current random seed.
- $V_{tsc}$ : MSE value for the TS model under the current random seed.

Table 4: Optimization Effectiveness Across Noise Types on the Exchange Dataset Using MSE as the Metric. This table displays the impact of various noise types and their optimized counterparts (NN for No Noise, GN for Gaussian Noise, GNO for Optimized Gaussian Noise, UN for Uniform Noise, UNO for Optimized Uniform Noise, TSN for Time Series Noise, TSNO for Optimized Time Series Noise) on forecasting accuracy at different prediction intervals (48, 96, 144, and 192 steps). The results demonstrate that our optimization methods consistently enhance model performance under each noise condition, validating their efficacy in reducing MSE across diverse perturbation scenarios.

		NN	GN	GNO	UN	UNO	TSN	TSNO
Exchange	48	0.043	0.058	0.052 ↓ <sub>-0.006</sub>	0.056	0.054 ↓ <sub>-0.002</sub>	0.102	0.073 ↓ <sub>-0.029</sub>
	96	0.086	0.111	0.091 ↓ <sub>-0.020</sub>	0.092	0.087 ↓ <sub>-0.005</sub>	0.131	0.104 ↓ <sub>-0.027</sub>
	144	0.124	0.146	0.126 ↓ <sub>-0.020</sub>	0.131	0.127 ↓ <sub>-0.004</sub>	0.175	0.141 ↓ <sub>-0.034</sub>
	192	0.175	0.213	0.176 ↓ <sub>-0.037</sub>	0.191	0.184 ↓ <sub>-0.007</sub>	0.239	0.178 ↓ <sub>-0.061</sub>

## E More Experiments

### E.1 Various Types of Perturbations

Table 5: Assessment of Optimization Effects on Various Noise Magnitudes Under Intermediate Layer Perturbations in the Exchange Dataset Using MSE as the Metric. The table compares the effects before (N for non-optimized) and after optimization (O) for Gaussian noise with standard deviations of 0.01, 0.02, and 0.03.

		0.01		0.02		0.03	
		N	O	N	O	N	O
Exchange	48	0.045	0.044 ↓ <sub>-0.001</sub>	0.051	0.046 ↓ <sub>-0.005</sub>	0.222	0.179 ↓ <sub>-0.043</sub>
	96	0.102	0.092 ↓ <sub>-0.010</sub>	0.116	0.098 ↓ <sub>-0.018</sub>	0.312	0.259 ↓ <sub>-0.053</sub>
	144	0.164	0.149 ↓ <sub>-0.015</sub>	0.181	0.153 ↓ <sub>-0.028</sub>	0.915	0.818 ↓ <sub>-0.097</sub>
	192	0.205	0.190 ↓ <sub>-0.015</sub>	0.259	0.215 ↓ <sub>-0.044</sub>	2.099	1.955 ↓ <sub>-0.144</sub>

Table 4 discusses the effectiveness of the FTS framework proposed in this paper in optimizing for Gaussian Noise, Uniform Noise, and Time Series Noise. Gaussian Noise is characterized by a mean of 0 and a standard deviation of 0.2. Uniform Noise ranges from 0 to 0.2 with a mean of 0.1. The magnitude of Time Series Noise is determined by multiplying the residuals obtained after sequence decomposition by a coefficient of 5. The table demonstrates that the method proposed in this paper exhibits robustness against various types of input perturbations. At a prediction length of 48, the impact of disturbances from the three types of noise is reduced by 40.00%, 15.38%, and 49.15%, respectively.



### E.2 More Intermediate Layer Perturbations

Table 5 evaluates the comparative effectiveness of optimization under varying degrees of intermediate layer perturbations in the Exchange dataset, measured using MSE as the metric. Gaussian noise with standard deviations of 0.01, 0.02, and 0.03 is incrementally introduced from left to right in the table. The comparative analysis reveals that the method proposed in this study exhibits robustness against noise in most cases. However, as the magnitude of the noise increases, the efficacy of the method gradually diminishes, with improvements becoming increasingly difficult to achieve.

### E.3 More Experiments about PGD Hyperparameters

Table 6: PGD Parameter Impact on MSE in the Exchange Dataset. This table evaluates the effects of step size (size) and the number of iterations (steps), noting that optimal results are achieved with specific settings.

		size	0.01	0.01	0.01	0.02	0.05
		steps	15	20	10	10	10
Exchange	48		<b>0.073</b>	0.076	0.090	0.076	0.089
	96		<b>0.104</b>	0.107	0.115	0.107	0.131
	144		<b>0.141</b>	<b>0.141</b>	0.139	<b>0.141</b>	0.142
	192		<b>0.178</b>	0.183	0.180	0.182	0.182

Table 6 discusses PGD parameters using MSE as the metric on the Exchange dataset, where size represents the step size for each iteration, and steps represent the number of iterations.

The comparison from the table shows that the best performance is achieved when size is 0.01 and steps are 15. It is worth noting that at a prediction length of 48, the performance is relatively poor with an size of 0.01 and steps of 10, resulting in a loss of 0.090. This may be due to the insufficient number of iterations, which fails to identify the weakest direction of perturbation. Similarly, when size is 0.05 and steps are 10, resulting in a loss of 0.089, the performance is also suboptimal. This could be because the larger step size per iteration makes it difficult to pinpoint a more vulnerable direction of perturbation.

Table 7: Optimization of Loss Function Parameters on the Exchange Dataset. Optimal settings are identified for  $\mathcal{L}_{snp}$ ,  $\mathcal{L}_{cps}$ , and  $\mathcal{L}_{sib}$ , highlighting the importance of specific constraints for improving MSE performance.

		$\mathcal{L}_{snp}$	1	0.5	1	1	1	1
		$\mathcal{L}_{cps}$	0.5	0.5	1	0.1	0.5	0.5
		$\mathcal{L}_{sib}$	0.05	0.05	0.05	0.05	0.01	0.1
Exchange	48		<b>0.073</b>	0.076	0.083	<b>0.073</b>	0.075	0.083
	96		<b>0.104</b>	0.109	0.133	0.111	0.106	0.129
	144		0.141	0.143	0.150	0.157	<b>0.139</b>	<b>0.139</b>
	192		<b>0.178</b>	0.184	0.184	0.211	0.180	0.180

### E.4 More Experiments about Regularization Parameters

Table 7 discusses loss function parameters using MSE as the metric on the Exchange dataset. It is observed that in most cases, the best performance is achieved when  $\mathcal{L}_{snp}$ ,  $\mathcal{L}_{cps}$ , and  $\mathcal{L}_{sib}$  are set at 1, 0.5, and 0.05 respectively. Constraints can improve model performance under certain conditions. For example, the performance of  $\mathcal{L}_{cps}$  deteriorates when set to 1 or 0.1, but is better at 0.5.

## F Introduction of Noise Perturbations

In our study, we utilize three distinct types of noise to investigate their impact on time series forecasting models, focusing on the effectiveness of the models under various noise conditions. These include residuals from the time series decomposition, as well as random noise generated from Gaussian and uniform distributions.

**Time Series Decomposition Residuals:** The Autoformer model utilizes a sequence decomposition approach that primarily separates the time series into trend components and residuals. These residuals are calculated as the differences

between the original time series values and the trend component. This representation isolates the stochastic variations in the data that are not explained by the identified trends, providing a distinct type of noise for analysis. Utilizing these residuals allows us to evaluate the robustness of our forecasting methods against the inherent randomness in the time series, independent of any long-term trend effects.

**Gaussian Noise:** Gaussian noise, or normal noise, is added to the time series data to simulate disturbances that follow a normal distribution, characterized by its bell-shaped probability distribution, defined by its mean and standard deviation. This type of noise is used to evaluate the model's capability to handle random fluctuations that exhibit statistical regularity, common in many real-world scenarios.

**Uniform Noise:** In contrast to Gaussian noise, uniform noise is generated from a uniform distribution, where each value within a specific range has an equal probability of occurrence. This introduces a consistent level of unpredictability across the specified range, testing the model's ability to perform under conditions of uniform random perturbations. It provides insights into the model's generalization capabilities across varied noise scenarios.

## G Visualization

In Figure 4, Figure 5, Figure 6 and Figure 7, we present the intermediate layers tensors of our model evaluated on the Exchange dataset using MSE as the performance metric. The prediction lengths are 48, 96, 144, and 192. Each heatmap represents different experimental conditions and their respective impacts on the model's performance.

**Base:** This represents the baseline scenario where no perturbations or optimizations are applied.

**Base + Per:** This heatmap shows the tensor under the influence of perturbations but without any optimization.

**Nper:** This heatmap is derived by subtracting the Base tensor from the Base + Per tensor, highlighting the noise introduced without optimization.

**Base + Opt:** This represents the scenario with optimization applied but without any perturbations.

**Base + Per + Opt:** This heatmap shows the tensor with both perturbations and optimizations applied.

**Oper:** This heatmap is derived by subtracting the Base + Opt tensor from the Base + Per + Opt tensor, highlighting the noise introduced with perturbations and optimization.

From the heatmaps, it is evident that the Oper heatmaps (perturbations with optimization) have significantly lighter colors compared to the Nper heatmaps (perturbations without optimization). This indicates that the noise introduced by perturbations is substantially reduced when optimization is applied. The lighter colors in the Oper heatmaps suggest that the model's intermediate layers are less affected by noise, demonstrating the robustness and stability imparted by the optimization process.

The comparison between Nper and Oper heatmaps clearly shows the effectiveness of the optimization in mitigating the adverse effects of perturbations. The method not only maintains the integrity of the intermediate layer outputs but also ensures that the overall model performance remains consistent. These visualizations affirm that our approach provides a significant performance advantage by reducing the susceptibility of the model to random noise, thus enhancing its robustness.

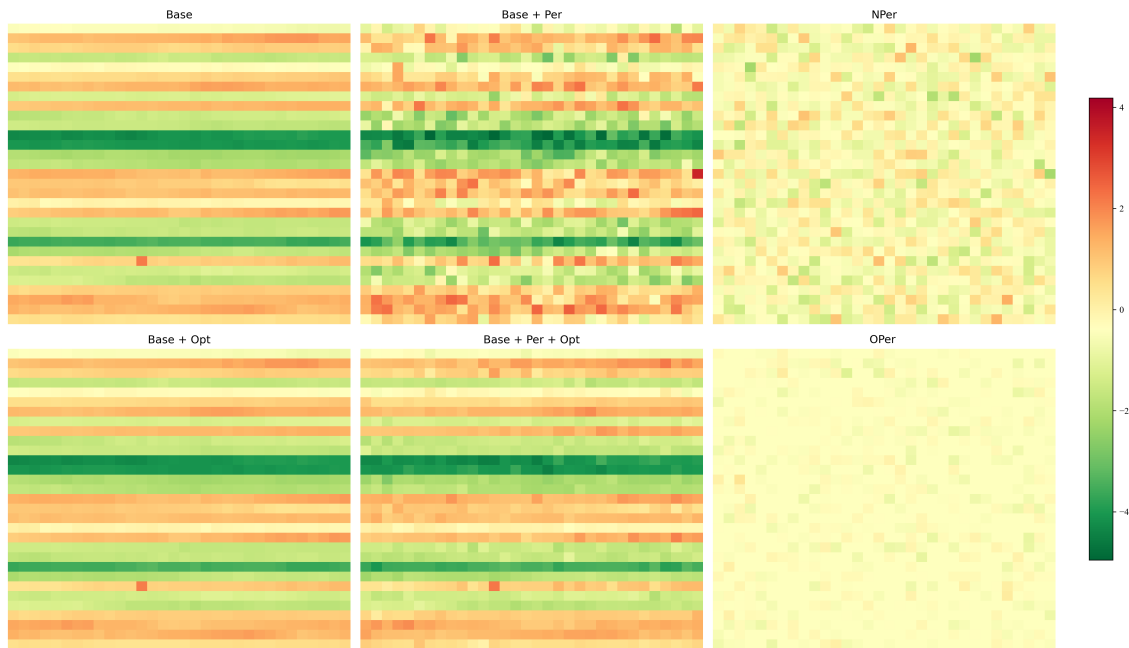


Figure 4: Heatmap for Prediction Length of 48.

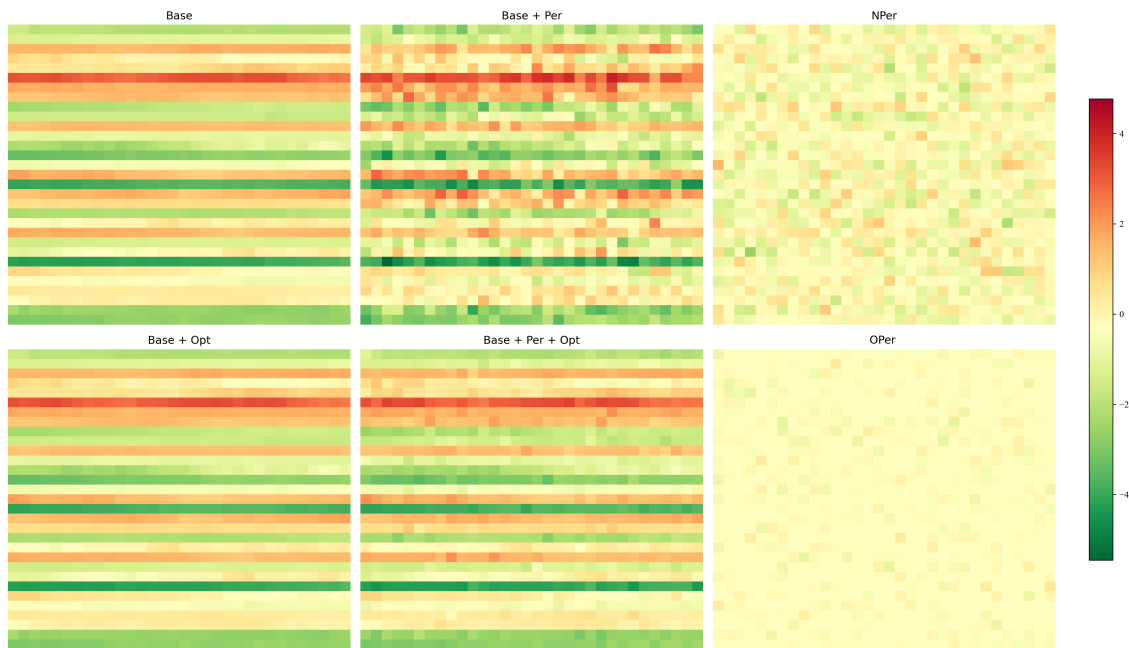


Figure 5: Heatmap for Prediction Length of 96.

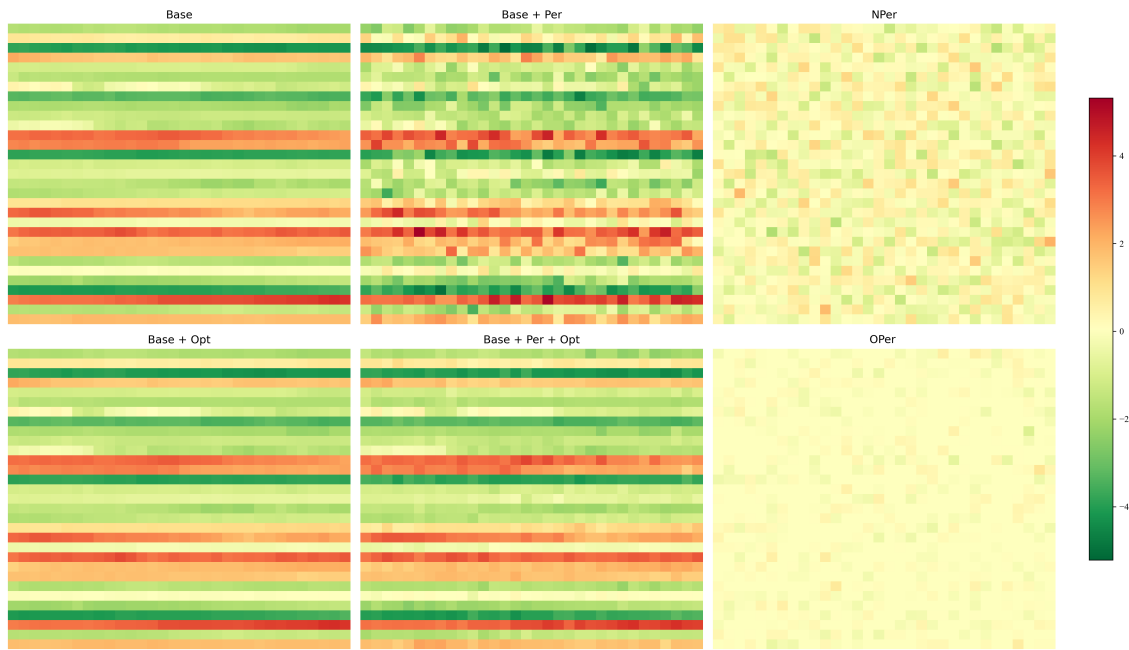


Figure 6: Heatmap for Prediction Length of 144.

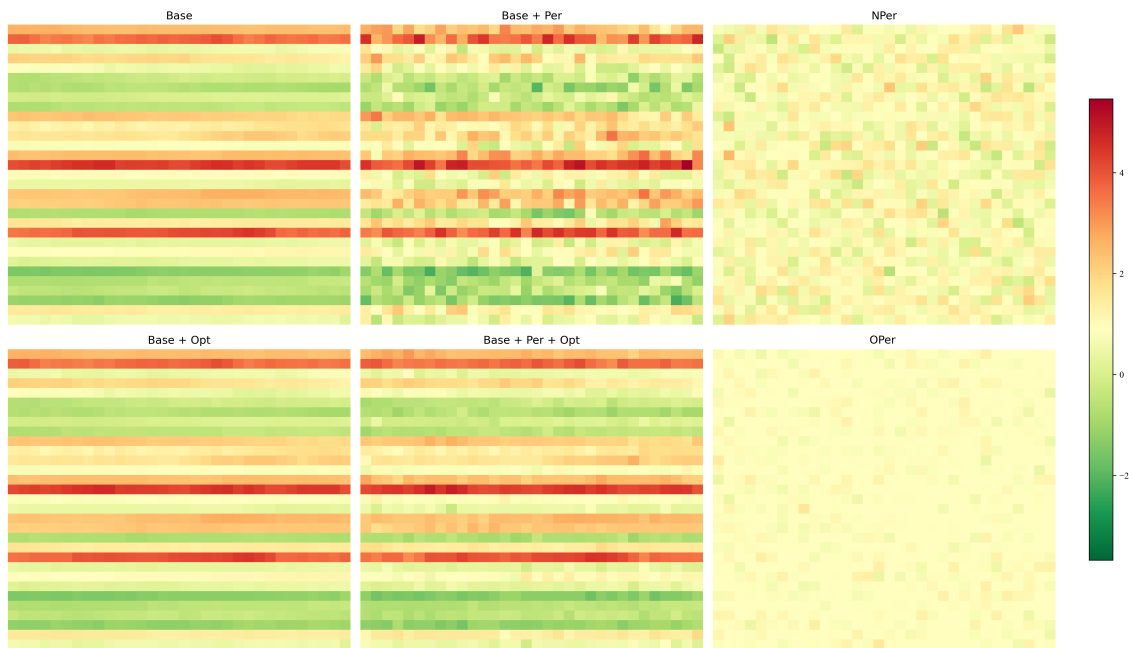


Figure 7: Heatmap for Prediction Length of 192.